Available online at www.eccomasproceedia.org
Eccomas Proceedia COMPDYN (2023) 1321-1336

ECCOMAS
Proceedia

COMPDYN 2023
9th ECCOMAS Thematic Conference on
Computational Methods in Structural Dynamics and Earthquake Engineering
M. Papadrakakis, M. Fragiadakis (eds.)
Athens, Greece, 12-14 June 2023

CASE STUDY: IMPACT OF ROUTE SPECIFIC LOADS AND NUMERICAL MODEL CALIBRATION ON FATIGUE ASSESSMENT OF AN EXISTING RAILWAY BRIDGE (COMPDYN 2023)

Stefan Lachinger[1], Sebastian Pissermayr[1], Marian Ralbovsky[1] and Alois Vorwagner[1]

[1]Austrian Institute of Technology GmbH
Giefinggasse 4
1210 Vienna, Austria
e-mail: {stefan.lachinger, sebastian.pissermayr, marian.ralbovsky, alois.vorwagner}@ait.ac.at

Abstract. *The presented case study investigates the proposed fatigue damage on an existing 108 year old riveted railway bridge, located in Austria. The bridge was instrumented with numerous sensors (strain gauges, inclinometers, temperature sensors) in the summer of 2022 and a Weigh in Motion (WIM) system was installed on the track. Since then continuous monitoring is carried out and the axle loads as well as the structural response of the structure during train passage is recorded. The study shows the process of numerical model calibration of a finite element (FE) model based on recorded sensor data and known defects of the bridge structure. The influence of the calibrated FE-model is shown by a comparison of calculated fatigue damage using measured loads from the WIM system as well as a train mix from codified design, both for the initial and the calibrated numerical model.*

Keywords: Railway, Fatigue, Weigh in Motion, Model calibration, Model updating, Monitoring

ISSN:2623-3347
Peer-review under responsibility of the organizing committee of COMPDYN 2023.
doi: 10.7712/120123.10479.21257

1 INTRODUCTION

Life time assessment with respect to fatigue failure of existing railway bridges is usually done to ensure safe operation for the remaining intended lifetime of the structure. Evaluation of fatigue damage usually includes large uncertainties. On one hand the resistance side, which, in civil engineering, is usually covered by S-N curves based on experiments including large scatter in the results. On the other hand, as fatigue is a cumulative damage, the load history of a structure is very important and information here is usually sparse. Also current load models from codified design are usually only intended for the design of new structures and very conservative for the assessment of existing structures. While actual loading on structures can be monitored by use of Weigh-In-Motion (WIM) systems, estimation of a structures load history is usually a challenging task. Uncertainty propagation of the uncertainties on the resistance, as well as on the loading and modelling side lead in general to overly conservative results from fatigue assessment. While the uncertainty on the resistance side is difficult to improve without destructive testing, a reduction of the uncertainties on the load and model side is usually possible with some effort and can help to improve the results of the assessment.

The presented case study focuses on an existing 108 year old riveted railway bridge, located in Austria. The bridge, which has some known defects, was instrumented with numerous sensors (strain gauges, inclinometers, temperature sensors) in the summer of 2022 and a WIM system was installed on the track. Since then continuous monitoring is carried out and the axle loads as well as the structural response of the structure during train passage is recorded.

The study shows the influence of numerical model calibration of a finite element model of the investigated bridge, based on recorded sensor data, as well as load models based on different levels of information on the proposed lifetime of the structure. Basic assessment is done with the load model from codified design while advanced assessment shows the influence of considering measured loads from the WIM system for actual loads.

2 Description of bridge used for case study

(a) View on the railway bridge

(b) Abutment wall pressing on the structure

Figure 1: Railway bridge used for case study

The bridge under consideration is part of the Austrian rail network and shown in Figure 1a. The cross-sections of the steel truss bridge consist of riveted steel plates and industrial sections.

As the investigated bridge is already more than 108 years old there are several signs of its age and defects: Cracks as well as applied constraints. As on one side the hillside is moving towards the bridge, the abutment wall behind the structure on the side of the fixed support has slowly deformed over the service life of the bridge. Now it presses against the last vertical upright of the left main truss and exerts a constraint on the bridge, see Figure 1b.
However, there are also signs of age in the rigidly constructed supports of the longitudinal girders, that extend over the main girders, see Figure 2a. Near these supports, material damage is observed in the form of cracks probably from bending of the main girder with its oblique supports, see Figure 2b.

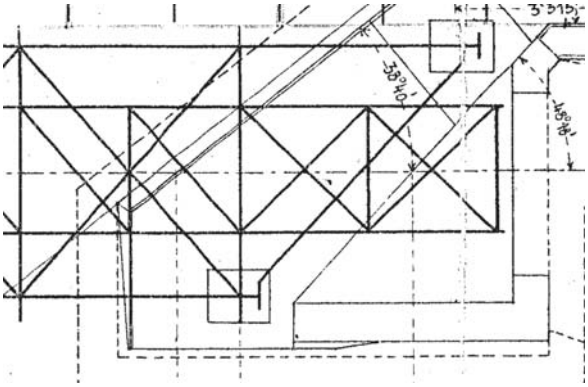

(a) Excerpt of plan overview

(b) Picture of crack at longitudinal girder support

Figure 2: Longitudinal girder extending over the main structure

The bridge is monitored using an extensive set of installed sensor. That includes a total of 69 strain gauges on the bridge, inclinometers, temperature sensors, laser distance measurements and a commercial Weigh-in-Motion (WIM) system installed on the structure that measures the axle loads, axle distances and train speeds of the traffic on the bridge.

3 Numerical Model and calibration process

A numerical FE-model is constructed. Figure 3 shows an sketch of the FE-model with the initial boundary conditions. The FE-model is constructed using beam elements for the main trusses and the longitudinal girder as well as shell elements for the cross girders.

As the goal of the calibration is the fatigue assessment of the structure the measured strains of the monitoringsystem are used for the calibration process instead of e.g. eigenfrequencies. Figure 4 shows the distribution of the strain gauges on the object of interest used for the calibration process. Blue and red marks strain gauges, whereas green marks points of interest for further calculations. Train data from the WIM system (axle loads, distances and train speeds) was used as loading for the calibration process.

Because the FE-model is updated in an iterative process, the numerical cost of the calculations are a relevant point to consider. To keep calculations simple, only influence lines (IFL) for a single passing normalized load are calculated with the FE-model and then the complete train response is calculated using superposition. The process of superposition using IFL is also described in Chapter 5.1.

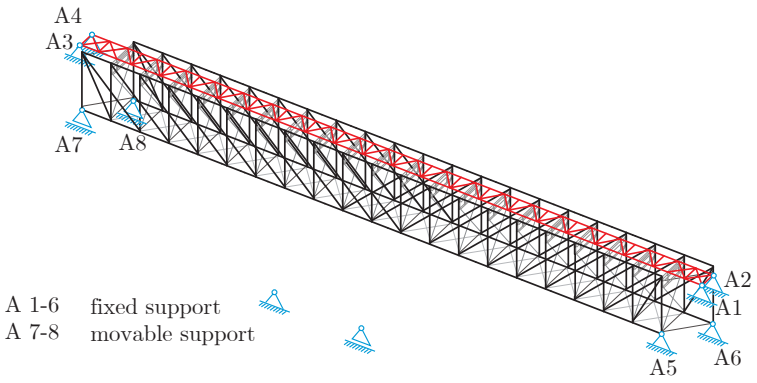

Figure 3: Sketch of numerical model with initial conditions

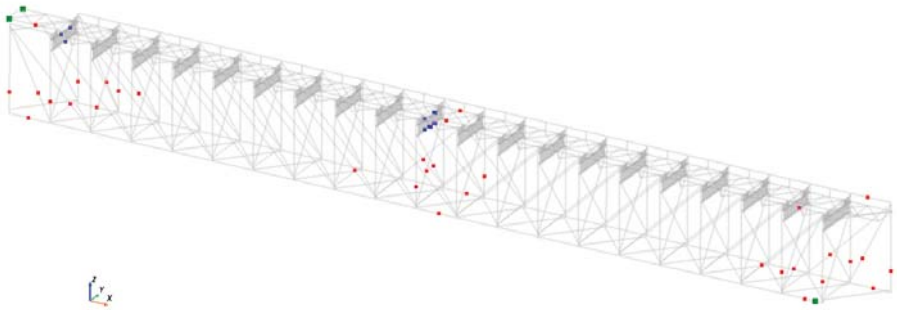

Figure 4: Position of strain gauges to measure data for modelupdating

3.1 Definition of Update Parameters

In the process of modelupdating, various parameters are defined in order to minimize the difference between measurement and calculation. The modelupdating method is often applied to concrete bridges because the elastic modulus of the concrete is a parameter that is subject to uncertainty. This is different for steel structures, where the stiffness represents a well known parameter (unless there is damage). The parameters of the optimization on the FE-model of a steel bridge are thus quite different from those on concrete structures. A parameter set is defined for the considered bridge, which mainly deals with boundary conditions. All parameters P1–P20, used for the calibration are displayed in Figure 5.

The definitions of the parameters P7-P16 are a special characteristic of the anaylized bridge. P7-P10 defines the pressure from the abutment wall, wheres P15-P16 consider damages of the cracked longitudinal girder, which are taken into account in the model in order to be able to evaluate the changes in the stress curves for train passes. P11-P14 are very specific parameters introduced due to the support design of the bridge. In order to obtain better results, also in the members close to the supports, this parameters are introduced according to figure 6. In particular, it is taken into account that a relative rotation of the two support elements can induce a displacement of the point of attachment of the support force. The effect can also be interpreted as stress resultant for variing stress distributions along the support edge. For different distributions of stress, the resulting force is not bound to act at the center of the support.

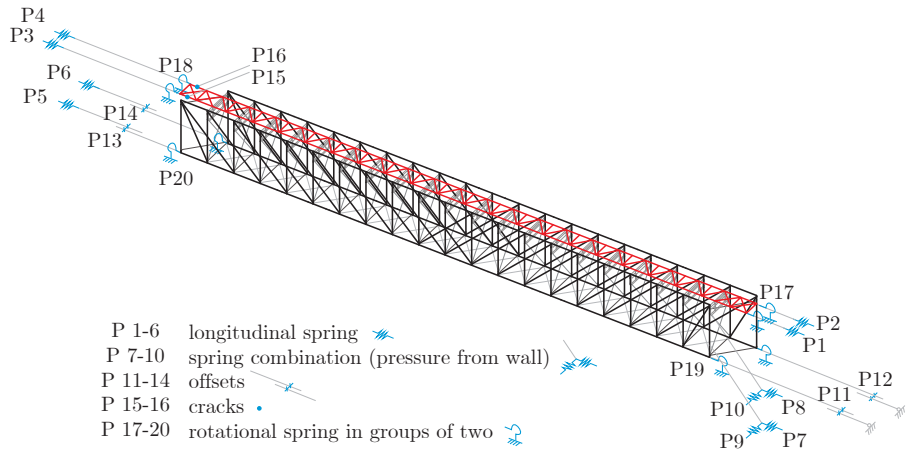

Figure 5: Identified Parameters of interest for the calibration process

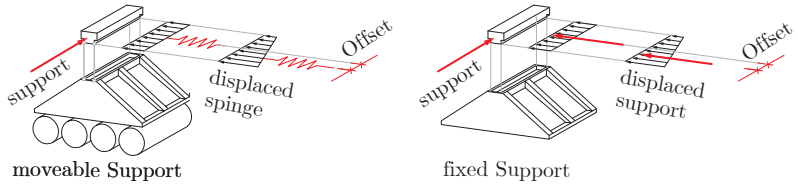

Figure 6: Introduction of Offset for horizontal support according to geometry

3.2 Update Process

When calibrating the model, calculated and measured data is compared. Basically, 3 sources of error are considered according to [1]:

Model structure errors occur when there is uncertainty concerning the governing physical equations.

Model parameter errors typically include the application of inappropriate boundary conditions and inaccurate assumptions.

model order errors arise in discretization of complex systems and can be considered to be a part of the model structure.

Under consideration of possible errors, the objective function $f(\theta)$ is introduced as single-objective function with a scalar output s given in eq. (1). Goal of the calibration process it to minimize $f(\theta)$. A simple approach using the squared error sum between measurement and calculation is chosen. Here, the error squares for all sensors and trains are not given extra weights. It should be noted that the number of calculated coordinates is directly proportional to the number of axes. Thus not trains but axes are equally weighted in the objective function.

$$f(\theta) = \sqrt{\sum_{t} \sum_{s} \sum_{j} \left(m(x_j, s, t) - M(\theta_i, x_j, s, t)\right)^2} \tag{1}$$

$M(\theta_i, x_j, s, t)$ is defined as Modell output for the vector of parameters θ_i, coordinates and sensor s and train t. $m(x_j, s, t)$ is defined as the measured data according to the bridge coordinate for a sensor s and train t. θ_i is a vector of the length p parameters for the values of the

parameters. x_j defines the jth coordinate from the coordinates of interest. i defines a iteration of the considered Parameters. j defines the index for the items of a list for all coordinates of the evaluated influence lines of a train. s defines the sensor of interest. t defines the train of interest. p defines the number of parameters parameters.

3.3 Calibration

The Nelder-Mead algorithm [3] is extremely well suited to the problem at hand, since firstly the calculation is only carried out with theory of 1^{st} order and secondly reasonable because bounds can be defined for the various parameters. E.g. the offset defined in figure 6 can be limited by the real size of the support.

The objective function for the optimization does not include all sensors. This is because strain gauges which measure very local effects and are especially located at the cross girder in the middle of the bridge, are considered to not be influenced by the change of boundaries. Hence the blue sensors in the middle of the bridge in figure 4 are neglected, because the level of detail in the FE-model shows much bigger importance on this sensors than the variation of boundary conditions.

In general, it is important to know what impact sensors have on the result and therefore the objective function. To quantify this, a simple approach defines the sensitivity s_p for a parameter of interest p_i and was introduced as follows in eq. (2).

$$s_p = \frac{|f(\theta(p_i = p_{i,max})) - f(\theta(p_i = p_{i,min}))|}{f(\theta)} \tag{2}$$

$f(\theta(p_i = p_{i,max}))$ is defined as objective function for the vector of parameters θ, where the parameter of interest p_i is as high as its upper boundary. The sensitivity describes the size of impact that the variation of the parameter has on the objective function. Here it is important to note that even parameters with a sensitivity $s_p < 1\%$ may have a significant impact on individual sensors, since in the objective function is formed by the sum over all points of the influence line, all sensors and all trains. The results of the sensitivity study are displayed in Figure 7. The parameters are listed on the x-axis, whereas measurements of different trains and also the sum for the trains are listed on the y-axis. In Figure 7a the objective function is related to the initial model, while in Figure 7b the objective function refers to the updated model. It can be seen that the parameters P1-P4 and P13, P14 have almost no influence on the model. While other parameters are not independent from each other and can also be quite relevant with a rather low sensitivity.

In the calibration process with the Nelder-Mead algorithm, an optimum is found after about 500–1000 iterations (depending on the respective start parameters). One iteration and thus the calculation of the IFL at 42 significant points, needs about 90 seconds. Thus an optimum for the defined 20 parameters in the calibration process takes about one day of computation.

In the results, and thus by comparing the initial (non-calibrated) model with the calibrated model, various effects can be detected. For this purpose, some sensors are shown in figure 8 for a passage of a single locomotive on the bridge. Sensor d-26 shows how by updating and defining the offset according to figure 6 can reproduce bending effects in the calibrated model. The good fit of strain gauge d-39 can be done mainly by the variation of the crack parameter P16 (see figure 5). The sensors d-48, d-52, and d-68 show rather global responses and a small amount of stress peaks. In this case, the improvement by optimization is only possible in a

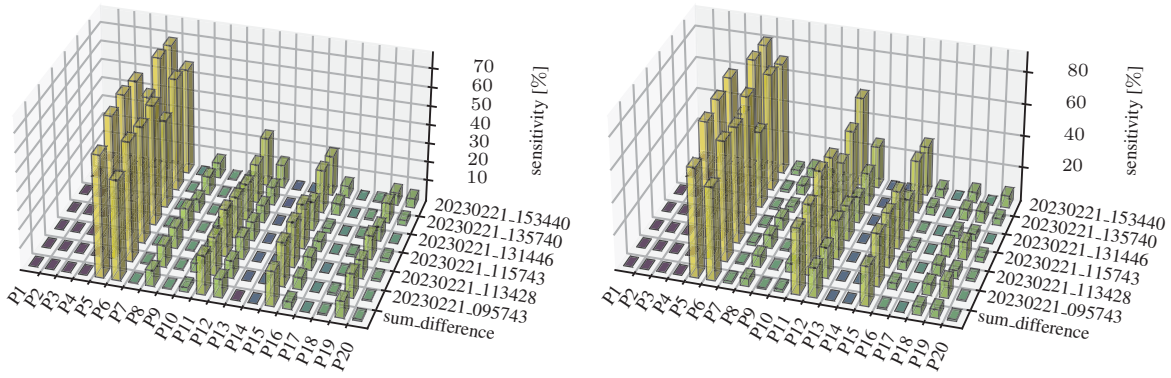

(a) Sensitivity on initial model

(b) Sensitivity on updated model

Figure 7: Sensitifity of update parameters on objective function

relatively small range, since the sensors are already well-matched anyway.

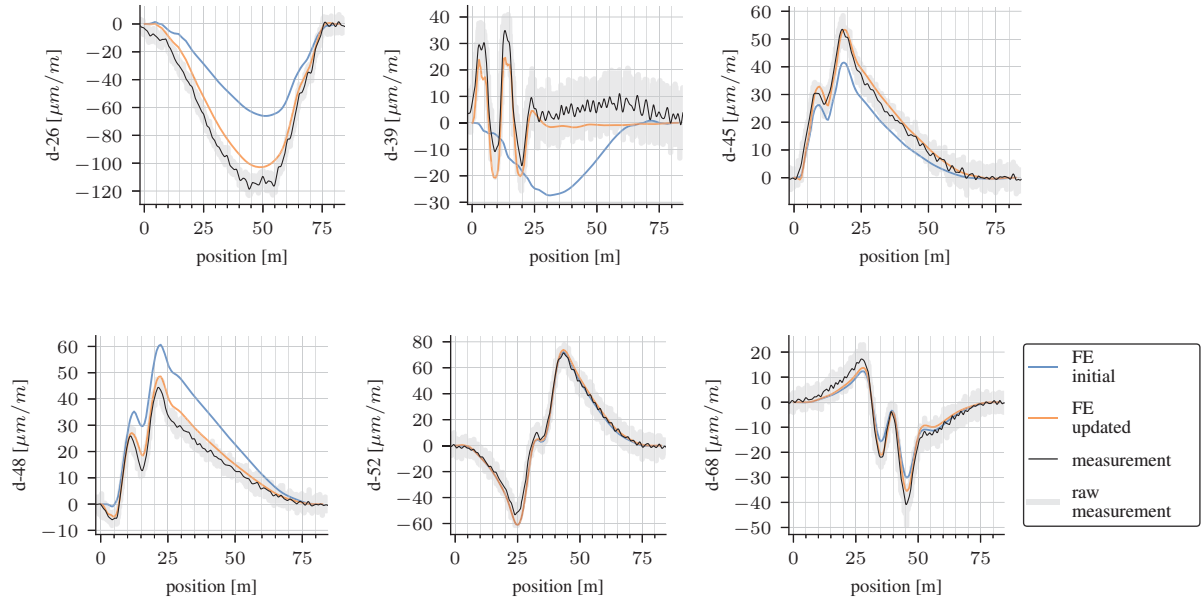

Figure 8: Comparison of results for initial and calibrated model at specific sensor position with measured data from a single locomotive passage

IFL for fatigue assessment are finally extracted at twelve positions at three different cross-sections shown in Figure 9. The positions are chosen to show big influence from the calibration process due to the deficits of the bridge structure from cracks in the longitudinal girder (cross-sections 1 and 2, see Figures 9a and 9b) and from the pressing abutment wall on one of the main trusses (crosssection 3, see Figure 9c). The global positions of the crosssections and the IFL positions are shown in Figure 9d

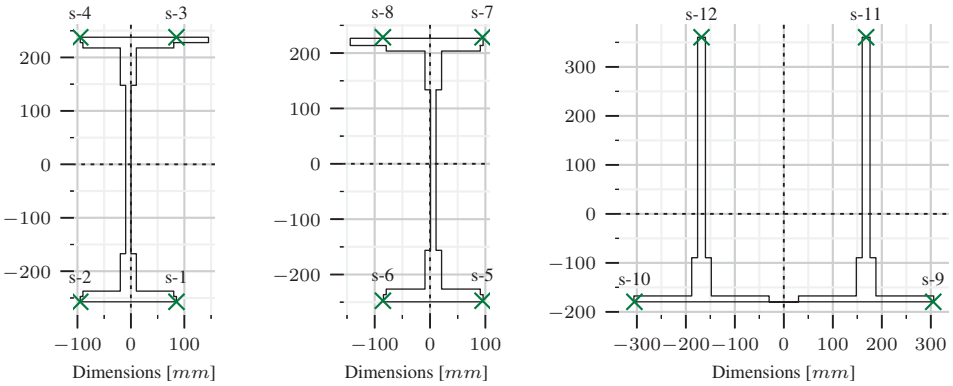

(a) Crosssection 1 (b) Crosssection 2 (c) Crosssection 3

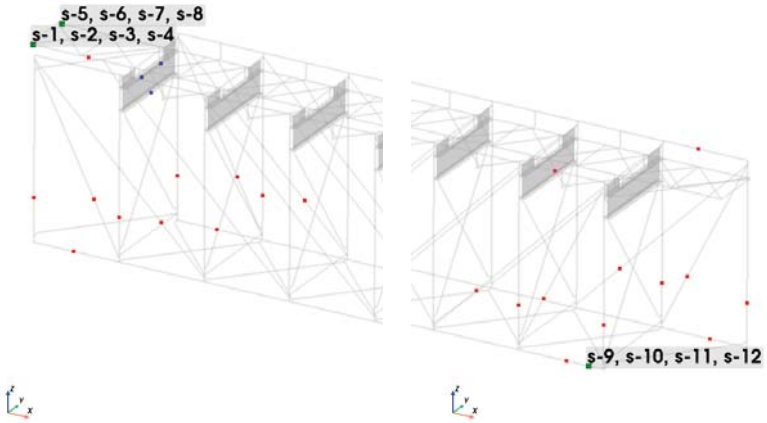

(d) Locations of crosssections on bridge

Figure 9: Positions used to extrac tIFL for fatigue assessment

4 Considered traffic

For the fatigue evaluation basically two different train load configurations are compared both for the initial and the calibrated model.

First load configuration is the fatigue load model for the standard traffic mix from EN 1991-2 [4] (EN-mix), as given in Table 1. For detailed axle load configurations please refer to [4].

The second load configuration consists of measured axle loads acquired with the installed Weigh In Motion system (WIM-data) on the bridge. Here measurement data for three months from September to November 2022 is used for the calculations. In Average 33.9 trains per day passed the bridge with a total yearly extrapolated volume of 3.673 million tons. This shows that the bridge is located on a track with little traffic compared to the EN-mix with a total yearly volume of 24.95 million tons. Figure 10 shows basic statistics of the measured trains. The majority of trains passed the bridge with a speed of 60 km/h with only a few outliers above the official speed limit on the bridge of 70 km/h. The majority of the relative train mass (Train Mass / Train Length) is rather low (around 2 tons/m) which indicates passenger trains. But

Train type	**Speed** $[km/h]$	**Train length** $[m]$	**Trains/day** $[-]$	**Mass of train** $[to]$	**Volume** $[10^6 to/year]$
1	200	262.10	12	663	2.90
2	160	281.10	12	530	2.32
3	250	385.52	5	940	1.72
4	250	237.60	5	510	0.93
5	80	270.30	7	2160	5.52
6	100	333.10	12	1431	6.27
7	120	196.50	8	1035	3.02
8	100	212.50	6	1035	2.27
Sum			**67**		**24.95**

Table 1: Standard traffic mix with axles $\leq 22.5t$ from EN1991-2 Annex D.3 [4]

also freight trains passed the bridge during the monitoring period, which can also be seen at the histogram for train length which shows trains up to a total length of around 700m.

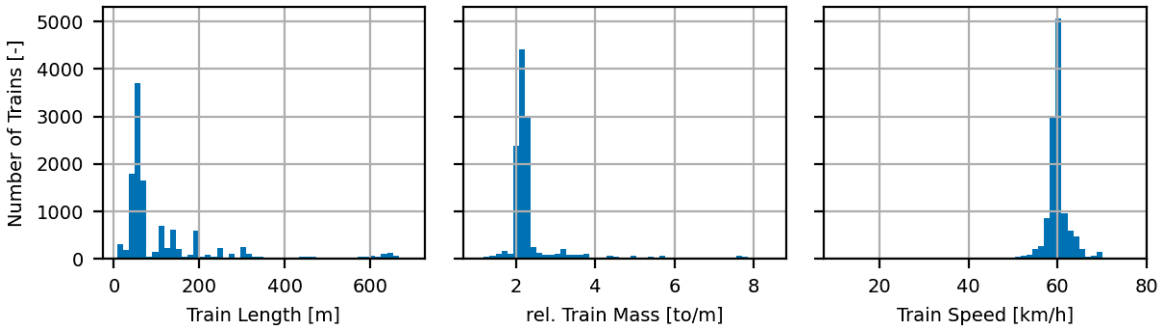

Figure 10: Histograms for train length, relative train mass and train speed for WIM data. Measured data extrapolated to a period of one year.

4.1 Analysis of traffic data

The trains measured with the WIM system are divided into passenger and freight trains. This is done using density based clustering (*DBSCAN algorithm from [5]*) with a chosen set of parameters with individual scaling. Also some additional constraints are used to further improve the results of the clustering algorithm. Trains that do not belong directly to the category of passenger or freight trains, as for example single or double locomotives, construction vehicles, etc. are assigned to the freight train category. Details of the clustering algorith are not disussed in this paper.

The results of the clustering algorithm are randomly checked for plausibility and show satisfying results, even if some outliers may exist. The clustering show that around 55 % of the yearly trains on the bridge are passenger trains and the remaining 45 % are freight trains. Figure 11 shows the results of the clustering algorithm for the WIM-data for train length against relative train mass. It can be seen, that the passenger trains are in very tight clusters compared to the freight trains which show a large scatter in the plotted parameter space. Figure 11 also shows the eight trains from the EN-mix as given in Table 1. Here train types one to four are passenger

trains and train types five to eight freight trains according to [4]. The comparison with the WIM-data shows that the EN-mix does not cover the whole parameter space of the real train traffic.

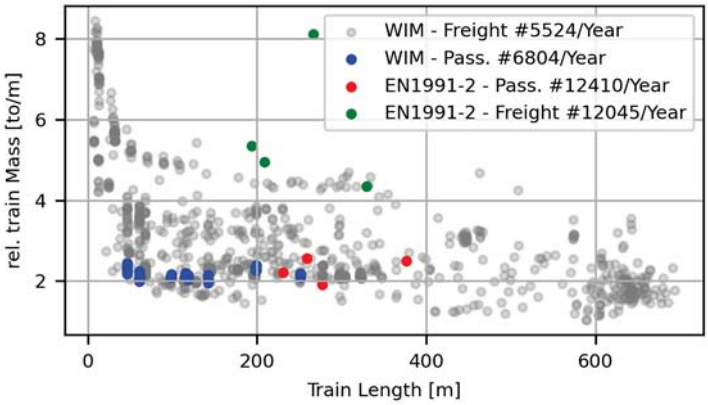

Figure 11: Results of clustering train traffic into passenger and freight train and comparison to standard traffic mix from [4]. Measured data extrapolated to a period of one year.

Table 2 compares the number of passenger and freight trains as well as the total yearly volume of the traffic (in million tons). The table shows that the WIM data gives a slightly higher ratio of passenger trains (55 %) than proposed the EN-mix (51 %) of the total number of trains. But the ratio of the total yearly traffic volume is compareable for EN-mix (31.5 % passenger trains) and WIM data (31.9 % passenger trains). The last two columns in Table 2 show the ratio of the respective values of EN-mix / WIM data. Here it can be seen that while the EN-mix proposes twice as much trains in total (24455 trains/year) than the WIM data (12328 trains/year) the total yearly traffic volume in tons is higher by the factor of 6.79 showing that the average train acc. to the EN-mix is heavier by the factor of 3.4 (3.69 for passenger and 3.13 for freight trains) compared to the WIM data.
The effect of the two different traffic mixes on the proposed fatigue life of the bridge is shown in Chapter 5.

	EN-mix		**WIM-data**		**EN-mix/WIM-data**	
	Nr. Trains [-]	**Volume [10^6 to]**	**Nr. Trains [-]**	**Volume [10^6 to]**	**Nr. Trains [-]**	**Volume [-]**
Pass. Train	12410	7.87	6804	1,17	**1.82**	**6.72**
Freight Train	12045	17.08	5524	2.50	**2.18**	**6.82**
Sum	**24455**	**24.95**	**12328**	**3.67**	**1.98**	**6.79**
Pass./Freight	**1.03**	**0.46**	**1.23**	**0.47**	**-**	**-**

Table 2: Comparison of basic metrics of EN 1991-2 Standard Traffic Mix and measured traffic with WIM system for a time period of one year.

5 Fatigue evaluation and comparison

This chapter brings together the results of the numerical model calibration as shown in Chapter 3 and the train load models of EN-mix and WIM-data as shown in Chapter 4. Comparison is done both for initial and calibrated model.

5.1 Train response by superposition of influence lines

Influence lines (IFL) are extracted for twelve positions in three cross sections as shown in Figure 9 both for the initial and the calibrated model. Figure 12 shows the resulting IFL for the three cross sections both for initial and calibrated model. It can be seen that the calibration process has quite a big influence on the chosen cross sections, especially for cross sections two and three. Here the calibrated model gives much higher amplitudes of the influence lines, indicating higher stresses during train passage and most likely higher proposed fatigue damage for the calibrated model.

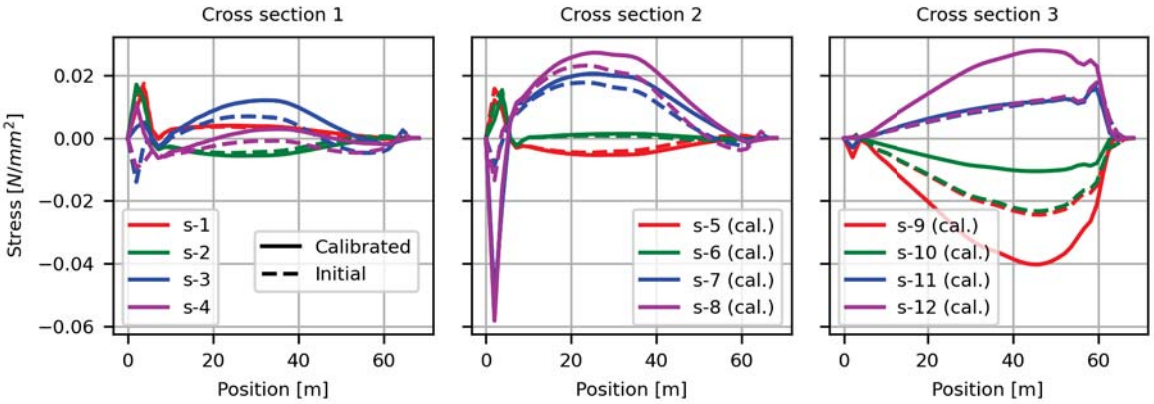

Figure 12: Extracted influence lines at the three considered cross sections both for initial and calibrated model

Dynamic amplification $\varphi(v, L_\Phi)$ is considered according to EN 1991-2 [4] Chapter D.1 with determinant length L_Φ for cross sections one to three as specified in Chapter 6.4.5.3 of [4] and the given (EN-mix) respective measured (WIM-data) train speed v. For cross sections one and two the determinant length is three times the cross girder spacing $L_{\Phi,CS1} = L_{\Phi,CS2} = 3 \cdot 3m = 9m$ and for cross section three the determinant length is the span width of the main girder $L_{\Phi,CS3} = 60m$.

For fatigue evaluation the train response $\sigma_{train}(x)$ for a train with n axles, axle positions x_i and axles loads F_i for an IFL is numerically calculated by superposition as given in Equation 3. Figure 13 shows exemplary calculated train responses, for one train acc. to EN-mix and one train taken randomly from WIM-data.

$$\sigma_{train}(x) = \sum_{i=1}^{n} F_i \cdot \varphi(v, L_\Phi) \cdot IFL(x_i - x) \tag{3}$$

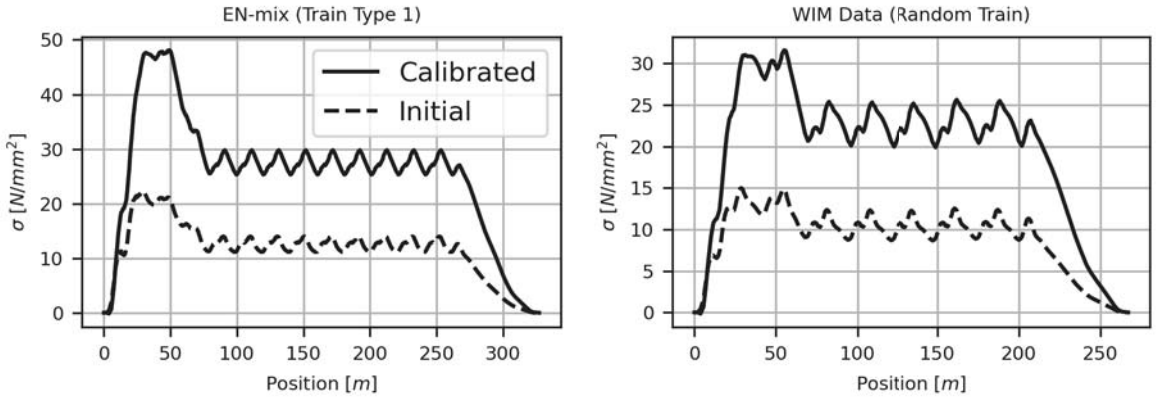

Figure 13: Examples of calculated train responses for initial and calibrated model by superposition of influence lines for position s-12. (Left) EN-mix Train Type 1; (Right) random train from WIM data

5.2 Calculating fatigue damage

A rainflow counting algorithm [7] is used to extract the k_j cyclic stress levels $\Delta\sigma_{i,j}$ (with $i = 1 \dots k_j$) out of the calculated response for each train j that passes the bridge in a time period of one year. For the riveted structure a detail category of $\Delta\sigma_c = 71\ N/mm^2$ (reference stress for $2 \cdot 10^6$ cycles) is used as given in the Austrian Code ÖNORM B4008-2 [6] Annex A.2.4. To consider the influence of the mean stress on the fatigue resistance of the riveted structure the permanent deadload stress σ_g of the bridge is calculated for each considered cross section position both for initial and calibrated model and the detail category is adjusted by the factor $f(\kappa_j)$ according to ÖNORM B4008-2 [6] Annex A.2.4.6. It has to be noted that the permanent deadload stress for the calibrated model has some uncertainties as the constrained stress due to the pressing abutment wall is unknown and can not be estimated in the calibration. κ_j is calculated according to Equation 4 with $\sigma_{min,Train,j}$ as the minimal absolute value and $\sigma_{max,Trainj}$ as the maximal absolute value from the train response including deadload stress. For calculation of κ_j the ratio is then calculated using the values with their real signs (not absolute).

$$\kappa_j = \frac{\sigma_{min,j}}{\sigma_{max,j}} = (\sigma_g + \sigma_{min,Train,j})/(\sigma_g + \sigma_{max,Train,j}) \tag{4}$$

The adjustment factor $f(\kappa_j)$ is calculated as given in Equations 5 and the adjusted detail category $\Delta\sigma_{c,adj,j}$ is calculated as given in Equation 6.

$$\begin{aligned} \text{if } \kappa_j < 0 : f(\kappa_j) &= \frac{1-\kappa_j}{1-0.40\cdot\kappa_j} \\ \text{if } \kappa_j \geq 0 : f(\kappa_j) &= \frac{1-\kappa_j}{1-0.60\cdot\kappa_j} \end{aligned} \tag{5}$$

$$\Delta\sigma_{c,adj,j} = f(\kappa_j) \cdot \Delta\sigma_c \tag{6}$$

Linear damage accumulation according to *Palmgren-Miner* [8] hypothesis is used for fatigue evaluation. ÖNORM B4008-2 [6] proposes an S-N curve with a constant slope factor of $m = 5$

and a cut off limit at $N = 3 \cdot 10^7$ load cycles (*Miner*-original). The cumulated damage of each single train $D_{train,j}$ is then calculated using the individual loadcycles $\Delta\sigma_{i,j}$ from rainflow counting and the linear damage accumulation rule [8] as given in Equation 7. Here $n_{i,j}$ is the calculated number of loadcycles for each $\Delta\sigma_{i,j}$ from rainflow counting and $N_{i,j}$ is the maximum bearable number of loadcycles for each $\Delta\sigma_{i,j}$. The yearly damage D_{year} is the sum of all single trains j passing the bridge in a period of one year. For better comparison of the results the damage sum is extrapolated to a 100 year period, as given in Equation 8. Fatigue failure is supposed to happen at a critical damage sum of $D_{crit} = 1$.

$$D_{train,j} = \sum_{i}^{k_j} \frac{n_{i,j}}{N_{i,j}} \tag{7}$$

$$D_{100} = 100 \cdot D_{year} = 100 \cdot \sum_{j} D_{train,j} \tag{8}$$

5.3 Comparison of proposed fatigue damage

Using the extracted IFL for the initial and the calibrated numerical model the proposed fatigue damage for a time period of 100 years is calculated as described in Chapter 5.2 for traffic taken from the EN-mix as well as from WIM-data. Calculation is done for all twelve detail positions s-1 to s-12 in the three considered cross sections, see Figure 9. As detail positions s-1 to s-6 result in zero damage (all load cycles below the cut off limit) they are not shown in the results. The calculations are summarized in Table 3 which shows the resulting values for the calculated 100 year damage sum $D_{100,pos}$ as well as some ratios for better comparison.
As seen in Table 2 the total yearly traffic volume of the EN-mix is higher by the factor of 6.79 compared to the measured WIM-data. To account for this and to compare the WIM-data with the EN-mix for the same total yearly traffic volume also results for a reduced EN-mix ($D_{100,red} = D_{100}/6.79$ is shown in Table 3. This represents the damage from the same combination of trains as in EN-mix, but with a reduced number of trains to match the total yearly volume in tons of the WIM-data.

Following the main observations from the calculations:

EN-mix Looking at the results for D_{100} it can be seen that already for the initial model very high damage sums of $D_{100,s-8} = 0.50$, $D_{100,s-9} = 0.78$ and $D_{100,s-10} = 0.62$ are calculated. For the calibrated model the positions s-8, s-9 and s-12 give damage sums exceeding our failure criterium of $D_{crit} = 1$ with $D_{100,s-8} = 2.06$, $D_{100,s-9} = 8.98$ and $D_{100,s-12} = 1.66$. For the positions s-10 and s-11 the damage sums were reduced for the calibrated model.
Looking at the ratio of the damage sums between calibrated and initial model it shows that the calibrated model gives about 71 times higher damage sum for s-12 then the initial model.

EN-mix (reduced) The results give respectively smaller damage sums compared to the standard EN-mix. Only for position s-9 the damage sum still exceeds D_{crit} with $D_{100,1-9} = 1.32$.

WIM-data With the measured load data the calculated damage sums are below D_{crit} both for the initial and the calibrated model. The maximum calculated value is for position s-9 of

		Cross Section 2		Cross Section 3			
Traffic	**Model**	**s-7**	**s-8**	**s-9**	**s-10**	**s-11**	**s-12**
EN-mix	**Init.**	1.4E-01	5.0E-01	7.8E-01	6.2E-01	1.9E-02	2.3E-02
	Cal.	6.0E-01	2.1E+00	9.0E+00	0.0E+00	1.7E-02	1.7E+00
EN-mix (red.)	**Init.**	2.1E-02	7.4E-02	1.1E-01	9.1E-02	2.8E-03	3.5E-03
	Cal.	8.9E-02	3.0E-01	1.3E+00	0.0E+00	2.5E-03	2.4E-01
WIM-data	**Init.**	5.7E-04	1.2E-02	2.1E-02	1.6E-02	5.6E-05	9.8E-05
	Cal.	1.4E-02	6.4E-02	3.3E-01	0.0E+00	5.0E-05	4.9E-02
EN-mix	**Cal./Init.**	**4.18**	**4.10**	**11.56**	**0.00**	**0.90**	**70.90**
WIM-data	**Cal./init.**	**24.16**	**5.43**	**16.00**	**0.00**	**0.89**	**502.12**
EN/WIM	**Init.**	**253.04**	**42.84**	**37.62**	**38.49**	**336.46**	**240.50**
	Cal.	**43.77**	**32.39**	**27.16**	**-**	**338.39**	**33.96**
EN(red)/WIM	**Init.**	**37.27**	**6.31**	**5.54**	**5.67**	**49.55**	**35.42**
	Cal.	**6.45**	**4.77**	**4.00**	**-**	**49.84**	**5.00**

Table 3: Comparison of 100 year damage sums for EN-mix and WIM-data both for initial (Init.) and calibrated (Cal.) numerical models. EN-mix (red) is the EN-mix calculated with the same yearly volume as WIM-data

the calibrated model with $D_{100,s-9} = 0.33$.
Looking at the reatio of the damage sums between calibrated and initial model it shows that for position s-12 the calibrated model gives a over 500 times higher damage sum then the initial model.

Ratio EN-mix/WIM-data Comparing the ratio of the damage sums for the EN-mix and the WIM-data shows that the EN-mix gives up to about 340 times larger damage sums compared to the WIM-data.

Ratio EN-mix (reduced)/WIM-data Comparing the ratio of the damage sums for the reduced EN-mix and the WIM-data, which represent the same yearly total traffic volume in tons still show up to 50 times higher damage sums for the reduced EN-mix copared to measured WIM-data.

These results show, that the EN-mix is much more aggressive with respect to fatigue damage than the real measured traffic on the bridge structure, even when reduced to represent the same yearly volume in tons. Also the partly very high ratios between calibrated and initial models show that due to the logarithmic definition of the S-N curve, changes in static system can lead to very high differences in proposed fatigue live of the structural details. The very large ratio for position s-12 (over 500) indicates that a high amount of individual load cycles were below the cut-off limit of the S-N curve for the initial model and exceeded this limit for the calibrated model. The comparison of the reduced EN-mix with the WIM-data also show that the EN-mix leads to much higher fatigue loads, even when reduced to represent the same yearly volume in tons.

6 Conclusions

An 108 year old existing railway bridge in Austria is extensively monitored. Both the structural response as well as the load impact by trains is measured. A detailled numerical finite element model is calibrated to the measured structural response and known damages of the

bridge structure are taken into account in the calibration. The numerical calibration process is described in detail in this work. The calibrated model shows, that the known damages have a significant, non neglectable, impact on the behaviour of the structure. For three considered cross sections that are highly affected by the calibration the influence lines are extracted from both the initial as well as the calibrated model and are used for fatigue assessment.

For the fatigue assessment different train configurations are considered. The standard traffic mix from codified design in the EN-1991-2 [4] as well as measured load data from monitoring. Fatigue assessment is carried out according to the Austrian guideline ÖNORM B4008-2 [6] that covers the assessment of existing bridge structures. Rainflow counting and calculation of the cumulated damage sum acc. to *Palmgren-Miner* is done and the resulting damage sums, extrapolated to a period of 100 years, are compared to each other.

It shows, that using the EN-mix safety with respect to fatigue failure can not be verified for the calibrated model, which is carefully calibrated with respect to existing damages of the structure. Also a reduced EN-mix, with adjusted total yearly volume in tons to match the measured volume does not proof fatigue safety for all considered positions of the structure. Using the real (extrapolated from three months of measurements) WIM-data allows the proof for fatigue safety for all the considered crosssections. The high difference of assessment using the reduced EN-mix and the WIM-data shows that the EN-mix is more aggressive with respect to fatigue compared to the real trains that pass the bridge. These shows that route specific fatigue load models, based on measurement data, are a very good tool for the fatigue assessment of exisiting and already damaged structures.

It has to be noted, that these comparisons are based only on actual measured loads and do not take historical data or prognosis on the evolution of traffic on the structure into account. Therefore the results are only of theoretical nature and have no evidence on the real fatigue life of the structure. For the specific bridge historical load data is obtained in an extensive research and results of fatigue evaluation taken this historical data into account will be published in the future.

Acknowledgments The study is carried out as part of Area 3.1 of the COMET Project Rail4Future, funded by the Austrian Research Promotion Agency FFG. The authors would like to thank the Austrian Federal Railways - Division ÖBB-Infrastruktur AG for making the project possible and for their continuing support.

REFERENCES

[1] J. Mottershead, M. Friswell, *Model Updating In Structural Dynamics: A Survey. Journal of Sound and Vibration - J SOUND VIB. 167. 347–375*, 1993.

[2] S. Ereiz, I. Duvnjak, J.F. Jiménez-Alonso, *Review of finite element model updating methods for structural applications*. Structures, Volume 41 684–723, 2022.

[3] Scipy Documentation of minimize function for the Nelder-Mead method. accessed 15 March 2023, `https://docs.scipy.org/doc/scipy/reference/optimize.minimize-neldermead.html`

[4] CEN - European Committee For Standardisation, *Eurocode 1: Actions on structures - Part 2: Traffic loads on bridges (EN1991-2*. CEN, 2003

[5] F. Pedregosa, G. Varoquaux, A. Gramfort, V. Michel, B. Thirion,O. Grisel,M. Blondel, P. Prettenhofer, R. Weiss, V. Dubourg, J. Vanderplas, A. Passos, D. Cournapeau,M. Brucher, M. Perrot, E. Duchesnay, *Scikit-learn: Machine Learning in Python*, `https://scikit-learn.org/stable`, 2023.

[6] Komitee 014, *ÖNORM B4008-2 Assessment of load capacity of existing structures - Part 2: Bridge construction*. Austrian Standards, 2019

[7] M. Matsuishi, R. Endo, *Fatigue of metals subjected to varying stress*, Japan Society of Mechanical Engineering, 1968

[8] M. A. Miner, *Cumulative damage in fatigue*, Journal of Applied Mechanics. 12: 149–164, 1945